A QUICK SEASONAL DETECTION AND ASSESSMENT OF INTERNATIONAL SHADEGAN WETLAND WATER BODY EXTENT USING GOOGLE EARTH ENGINE CLOUD PLATFORM

S. M. Seyed Mousavi[1], M. Akhoondzadeh[1,*]

[1] School of Surveying and Geospatial Engineering, College of Engineering, University of Tehran, Tehran, Iran - (mortezamousavi, makhonz) @ut.ac.ir

Commission IV, WG IV/3

KEY WORDS: GEE, MNDWI, Shadegan Wetland, Sentinel-2, histogram analysis, random forest.

ABSTRACT:

Understanding the variation of Water Extent (WE) can provide insights into Wetland conservation and management. In this study, inter-and inner-annual variations of WE were analyzed during 2019–2021 to understand the spatiotemporal changes of the International Shadegan Wetland, Iran. We utilized a thresholding process on Modified Normalized Difference Water Index (MNDWI) to extract the WE quickly and accurately using the Google Earth Engine (GEE) platform. The water surface analysis showed that: (1) WE had a downward trend from 2019 to 2021, with the overall average WE being 1405.23km²; (2) the water area reached its peak due to the water supply to International Shadegan Wetland through the Jarahi River and upstream reservoirs at the end of 2019 and the beginning of 2020, and the largest water body appeared in Winter 2019, reaching 1953.31km². In contrast, the smallest water body appeared in Autumn 2021, reaching 563.56km²; (3) The WE of the wetland showed predictable seasonal characteristics. The water area in Winter was the largest, with an average value of 1829.1km², while it was the smallest in Summer, with an average value of 1100.3km²; (4) The average water area in 2019 was 1490.5km² whereas in 2020 and 2021 decreased by 9% and 25%, respectively, and reached 968.6km² and 811.9km². Finally, to evaluate the proposed model, its results were compared with the Random Forest (RF) classification results. Accordingly, Histogram Analysis (HA) classification achieved 94.6% of the average overall accuracy and the average Kappa coefficient of 0.93, but the RF method obtained 95.38% of the average overall accuracy and an average Kappa coefficient of 0.94.

1. INTRODUCTION

Remote sensing (RS) is a quickly growing technology that provides inexpensive and trusty information for environmental changes at different scales, also it can provide data long-collected repeatable, and even real-time (Magsar et al., 2021). The use of remote sensing (RS) data is a good option for monitoring and mapping dynamic surface water areas such as wetlands. Wetlands are worth ecosystems and offer substantial services to both nature and human beings. For example, they are essential to water purification, carbon cycles, flood and storm control, soil erosion control, and providing wildlife habitats (Fekri et al., 2021). These valuable resources have undergone drastic changes due to climate change and increasing human activities (Seyed Mousavi and Akhoondzadeh Hanzaei, 2022). The high rate of wetland loss during the 20th and 21st centuries has resulted in a global wetland decrease of 64-71% since 1900 (Adeli et al., 2022). The wetland area is an important indicator of climate change and is related to climatic factors that are critical for understanding the mechanisms that control changes in water levels (Kang et al., 2015).

Although deep learning (Aghdami-Nia et al., 2022; Rostami et al., 2022b) and machine learning (Ranjbar et al., 2021; Rostami et al., 2022a) algorithms are popular in many RS fields, conventional methods are still used effectively. variant methods, such as single-band density cutting (Work and Gilmer, 1976), and spectral water indexes (Hui et al., 2008; Li et al., 2016), were improved to extract water bodies from different remote sensing images. Amongst all existing water body mapping methods, the index-based methods are kinds of reliable method, because it is user-friendly, efficient, and has a low computational cost (Ryu et al., 2002). Index MNDWI, In the last few years, has been broadly applied to produce water body maps at various scales. For example, Carroll et al. produced a new global raster water mask with used MODerate-resolution Imaging Spectroradiometer (MODIS) images which have a 250-m spatial resolution. (Carroll et al., 2009). Li et al. estimated the Spatiotemporal Changes in Major Lake Surface Areas in Arid Xinjia between 2000 and 2014 with MODIS images. (Li et al., 2015). Huang et al. illustrated water body variations using long-term MODIS data time series (Huang et al., 2012). Ma et al. Ma et al. used the Spatial and Temporal Adaptive Reflectance Fusion Mode for studying Dynamic changes of wetland resources based on MODIS and Landsat image data fusion. For small-scale studies like regional studies, image collection Landsat is the popular dataset. For example, Hui et al. modeled the spatiotemporal change of Poyang Lake using multi-temporal Landsat TM and ETM+ images (Hui et al., 2008). Gao et al. By using Cross-Fused-Based and Normalized Difference Index Analysis, it was able to extract wetland changes from Multitemporal Landsat 8 OLI images. (Gao et al., 2018). Yang et al. monitored Spatial and Temporal Changes in the Dongting Lake Basin of China from 1990 to 2020 using Landsat TM/ETM Remote Sensing Images (Yang et al., 2022). Emami and Zarei did modeling Lake Urmia water's surface changes using Landsat TM/ETM Remote Sensing Images (Emami and Zarei, 2021). Rokni et al. recognized change using Landsat TM, ETM+, and OLI images (Rokni et al., 2014). Mousavi et al. used Landsat OLI images between 2000 and 2019 to Monitoring and Prediction the changes in the water zone of the Anzali Wetland (Seyed Mousavi and Akhoondzadeh Hanzaei, 2022). Wang, et al. identified water features and detected inter-and inner-annual variations of the Water Extent

* Corresponding author

from 1978 to 2020 using Landsat TM, ETM+, and OLI images (Wang et al., 2022).

The Landsat images have better spatial resolutions than MODIS, which can help us extract open water bodies with more explicit and accurate boundaries. also, these images don't have enough spatial resolution to identify smaller-measure water bodies. moreover, by following out remote sensing images, like IKONOS, and Quick-bird, which are fine spatial resolution images these small-sized water bodies extend can be mapped. but these images have no SWIR band, building it impossible to use the MNDWI method.

In recent years, the Google Earth Engine (GEE) platform has been widely used. This platform integrates a massive mount of remote sensing data and has the benefit of fast processing and analysis of spatial data. For example, used 3 million Landsat remote sensing images from 1984 to 2015 using the GEE platform to produce a global water distribution map (Pekel et al., 2016). Deng et al. used 75,593 Landsat remote sensing images from 1984 to 2015 to monitor the dynamic changes in open surface open water in the Yangtze River Basin in China using the GEE platform. Mousavi et al. used Landsat images to Monitoring of the monthly changes in the water of wetlands from 2000 to 2019 using the GEE platform (Seyed Mousavi and Akhoondzadeh Hanzaei, 2022) therefore, the GEE provides us with a new insight to understanding the long-term changes in the wetland surface area (Jiang et al., 2021).

In recent years, the water surface of International Shadegan Wetland (ISW) has changed. This study considers the feasibility of Sentinel-2 data and has been carried out to extract the water area of the ISW using a relatively simple, efficient, and accurate method. Therefore, this research uses the image classification method based on the Histogram Analysis (HA) of MNDWI images. Particularly we aimed to achieve the following goals: (1) developing an automatic water extraction framework using Sentinel-2 images and the HA based on the GEE platform, and (2) utilizing an object-oriented Random Forest (RF) algorithm for the wetland classification based on the GEE platform, (3) comparing results ways HA and RF algorithm, (4) analyzing the WE change of ISW Lake from 2019 to 2021, and (5) exploring the spatiotemporal characteristics of the ISW extent and discussing the causes of the changes in ISW on an annual and seasonal basis.

2. MATERIALS

2.1 Study Area

The study area was one of the most important Iranian Ramsar Sites located, is placed within the province of Khuzestan in southwestern Iran (Figure 1). the ISW at the foremost downstream reach of Jarrahi river covers an approximate area of 5377km² (29◦300–31◦000 E and 48◦20’–49◦100 N) at the north end of the gulf which is restricted by the towns of Mahshahr Abadan, and Shadegan (Almasi et al., 2020). The ISW plays an important hydrological and ecological role within the natural functioning of the northern Gulf, and the economic situation for residents and acts as an enormous barrier to the entry of dust from the deserts of neighboring countries (Fekri et al., 2021).

Shadegan wetland represents a singular wetland along the Persian Gulf that is includes vast areas of reed beds, open water, mudflats, estuaries, Khur Musa bay, isolated small islands, and shorelines along the Persian Gulf. due to such habitat diversity, it provides globally significant ecological services.

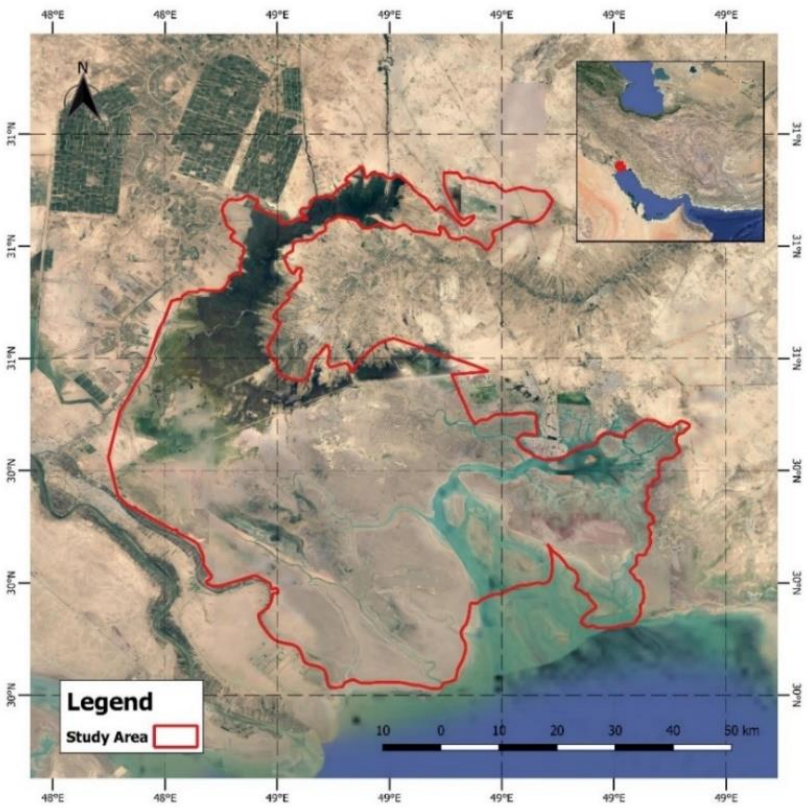

Figure 1. The geographical extent of ISW and its surrounding areas, located in southwestern Iran, and the wetland boundary, are outlined in red.

2.2 Dataset and Pre-Processing

Evaluating the short-term of the ISW utilized Sentinel-2 MSI satellite images which this collection of satellite images provided by the European Space Agency (ESA). they presented a Level-2A orthorectified product that surface reflectance corrected using the Sen2Cor algorithm. we used 365 free-of-cloud images together with a 5-day temporal resolution available from 21 March 2019 to 20 March 2021.

The study area (Figure 1) is generally contained by open water, soil, and vegetation specifications. Therefore, for better extraction and separation of water area from other features of the region, the MNDWI index was calculated for each season. we considered the SWIR band (B11) and Green band (B3) which have 20m and 10m spatial resolution resampled to 20m to be employed within the MNDWI composition.

The reflection of buildings typically increases from the infrared near the SWIR band, which Xu used instead of the NIR band to suppress buildings that are easily mistaken for water in NDWI thanks to the near-infrared band (Xu, 2006). He was ready to effectively suppress the noise of the building to increase the degree of water. supported this finding, the MNDWI was proposed, which is defined as Equations (1):

$$MNDWI = \frac{\rho_{Green} - \rho_{SWIR}}{\rho_{Green} + \rho_{SWIR}} \quad (1)$$

where ρ_{Green} = Green band

ρ_{SWIR} = SWIR band

Water bodies generally attract more SWIR light than NIR light which causes water bodies to have greater positive values in MNDWI than NDWI; vegetation, soil, and built-up classes have smaller negative values because they reflect more SWIR light than green light (Sun et al., 2012).

Satellite	Spectral Resolution (μm)	Spatial Resolution(m)	Number of Images Used
Sentinel-2 MSI (2019–2021)	13 Band	B2, B3, B4, B8: 10 m; B5, B6, B7, B8A, B11, B12: 20 m; B1, B9, B10: 60 m;	635

Table 1. Detailed information of satellite images used.

3. METHODOLOGY

The flow diagram of wetland water level analysis in this study is shown in Figure 2. This diagram consists of five sections: The first, second, third, and fourth sections respectively introduce the remote sensing data of this study, image pre-processing, extract, and Histogram Analysis and classification in GEE. The fifth section mainly analyses changes in the water area. Details are explained in the following sections.

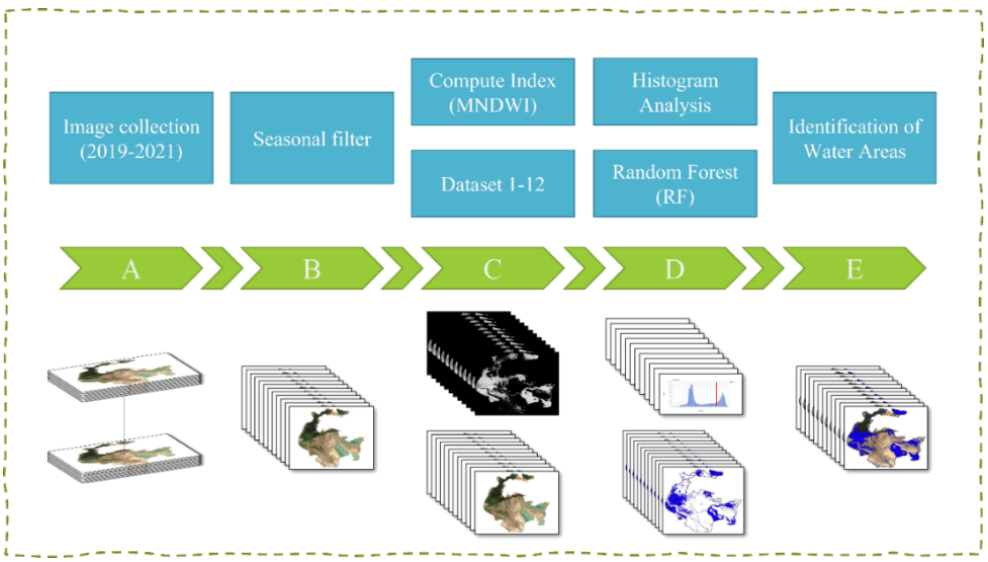

Figure 2. Flowchart of the study of water surface changes ISW in Iran with Google Earth Engine.

3.1 HAC

In this study, changes in the water level of ISW were investigated using multispectral images of Sentinel-2 (MSI) between 2019 and 2021 in the GEE system. GEE provides a system for fast access to large volumes of satellite imagery in a systematic and reproducible manner. This platform provides different data catalogs with various features including various weather data and satellite-based measurement systems at different wavelengths, both optical and non-optical, environmental variables, weather and weather forecasts, and land cover collection that can use for studies related to the earth. (Gorelick et al., 2017). Due to the coding environment that is embedded in this system, it is easy to call a large volume of different images and data, and due to the high processing power of the system, the desired operation can be performed online on the system itself and the final output can be extracted in various formats. All the processing steps performed in this study are shown in the methodology diagram presented in Figure 2. A 10% cloud filter was applied to Sentinel-

2 images and since there is no single algorithm for Sentinel-2 images, the median algorithm was used to analyze the seasonal time series. MNDWI was applied to the composite images to extract water levels.

After generating MNDWI, water bodies can be mapped using a suitable threshold value with a simple segmentation algorithm. In general, we use zero thresholds in MNDWI to separate the water body from other features. however, multispectral images obtained by different satellite platforms in different regions and at different times always have different attributes. Therefore, we should choose the threshold according to the characteristics of each MNDWI image. Then, using the histogram of each MNDWI image and determining the optimal threshold on the histogram, blue mask images were created.

3.2 RFC

Nowadays, RF is one of the most commonly used algorithms of machine learning for land cover classification using remote sensing data, by attention to, an analysis of 349 GEE peer-reviewed articles over the last 10 years, the RF algorithm is the most frequently used classification algorithm. (Tamiminia et al., 2020).

According to Noi Phan et al. (2020), the reasons for RF using considerable interest over the last two decades are (1) Good management of the outliers and noisier datasets; (2) Good performance against multi-dimensional datasets; (3) earning better precision than other common classifiers, such as KNN, SVM or MLC in many applications; and (4) boosting the processing speed and relieve time by selecting key variables. Considering all these reasons, we select RF for the present study, the RF Algorithm prepared in the Google Earth Engine system was used to classify the wetland. We used GEE for two steps, the first making the RF Algorithm classification framework, then gathering all Sentinel-2 imagery for the study area and preparing the training data.

We created twelve datasets on the GEE platform with respect to the studied seasons. Dataset 1 to Dataset 12 are median imageries, these datasets, have the same spatial resolution (20m).

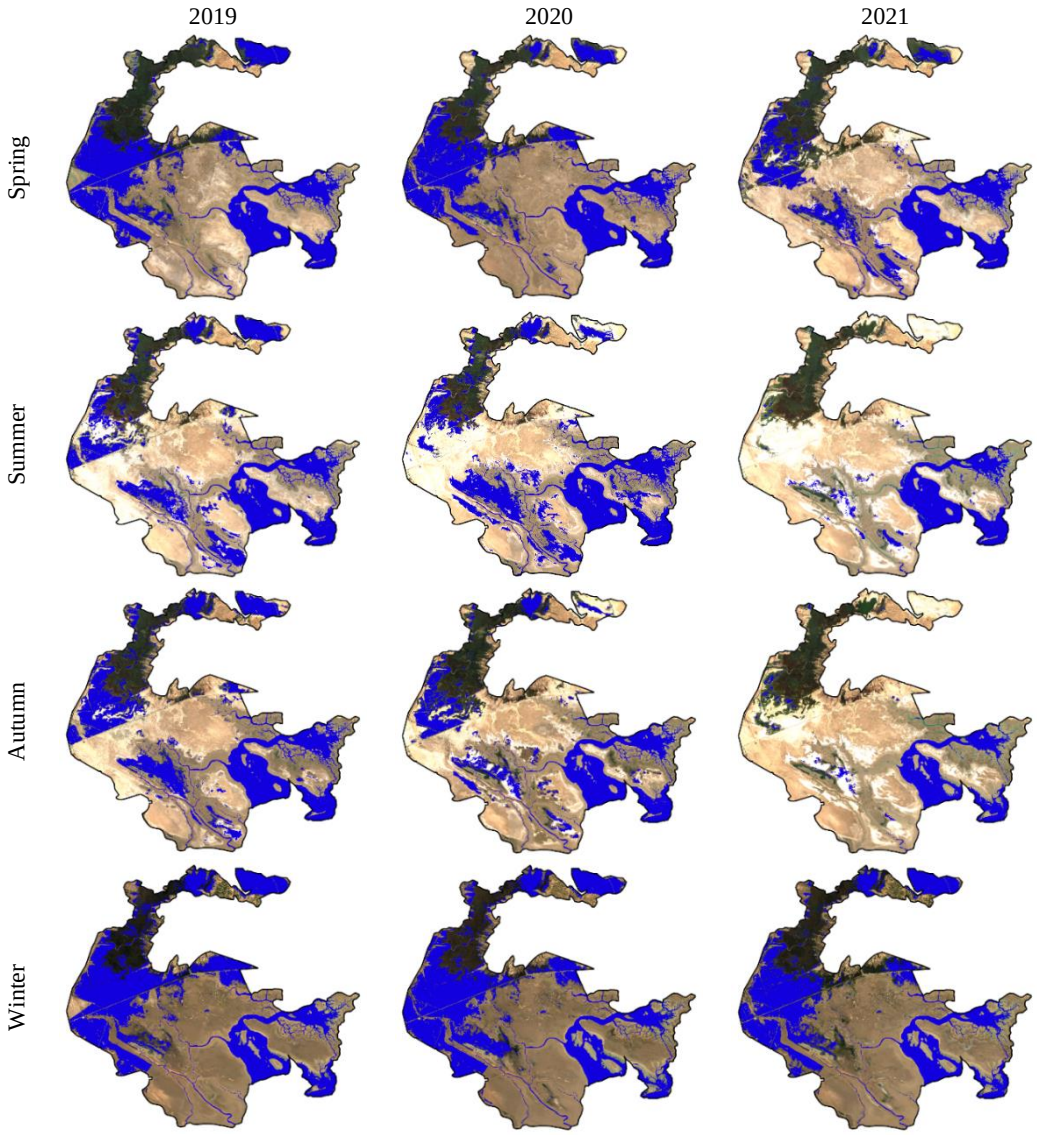

Figure 3. The seasonal surface water body distribution of ISW from 2019 to 2021. According to the Figures, water bodies are scattered mainly in the eastern and western parts of ISW, regardless of the different seasons of the year, while they are smaller in the central areas.

4. RESULTS AND DISCUSSION

4.1 Comparison and model performance evaluation

We applied the same training sample and validation data points to classify and determine the accuracy of the land cover maps. As mentioned within the Methods section, other than the spectral bands of Sentinel-2 images, we also used additional variables to boost the accuracy of the land cover maps. As is evident from Table 2, the typical water body area for 3 years derived from the HA classification was 1405.23km² and for the RF was 1287.18km².

Methodology	Area (km²)
HA Classification	1405.23
RF Classification	1287.18

Table 2. Water bodies areas.

Analyzing the results of the Accuracy Metrics for Evaluating Results table (Table 3), HAC achieved 94.6% average overall accuracy (OA), an average Kappa coefficient of 0.93, an average F1 Score of 94.50, and an average Recall Score of 94.40 but RF classifier obtains 95.38% average OA, average Kappa coefficient of 0.94, average F1 Score of 95.53, and average Recall Score of 95.47.

Metrics	RF	HA
OA (%)	95.38	94.60
Kappa	0.94	0.93
F1 (%)	95.53	94.50
Recall (%)	95.47	94.40

Table 3. Accuracy Metrics for Evaluating Results

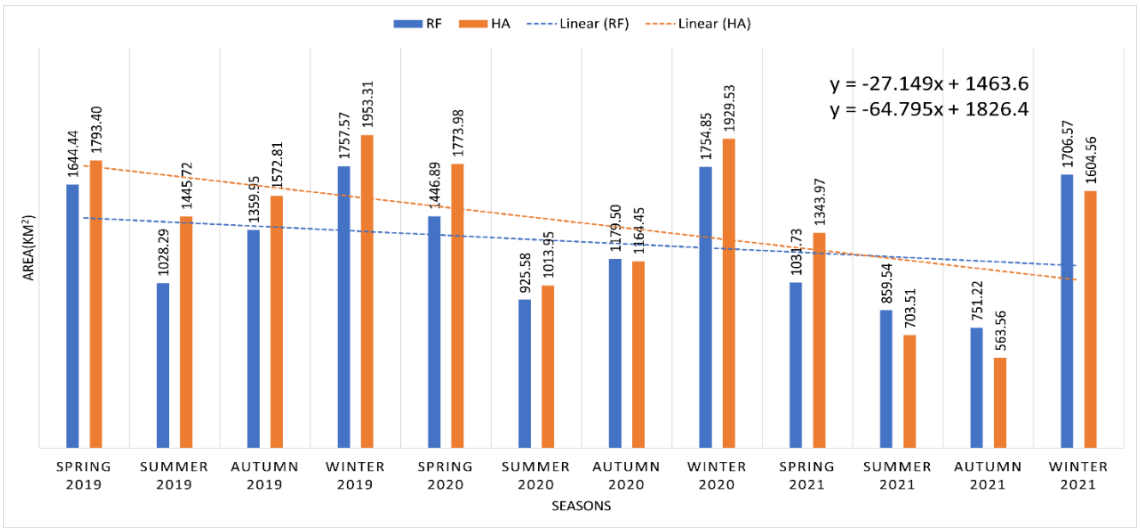

(a)

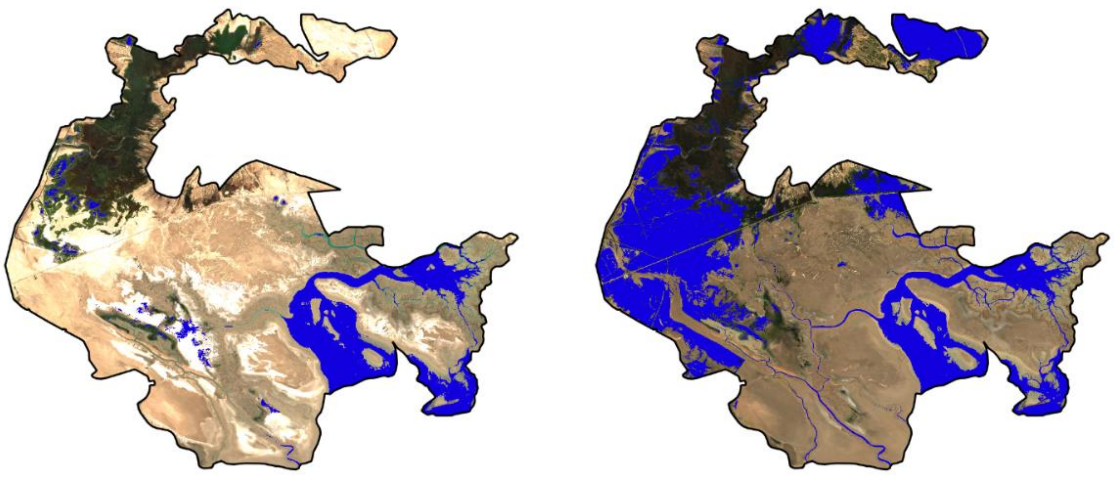

(b) (c)

Figure 4. Variations in the water area of ISW during 2019-2021: (a) Mean water area changes in ISW for each season from 2019 to 2021. and (b) Minimum and (c) Maximum WE of ISW in this study.

This contribution has been peer-reviewed. The double-blind peer-review was conducted on the basis of the full paper.
https://doi.org/10.5194/isprs-annals-X-4-W1-2022-699-2023 | © Author(s) 2023. CC BY 4.0 License.

4.2 The WE change of ISW from 2019 to 2021

The general water changes of ISW have distinct annual and inter-year characteristics in the period 2019 to 2021. The version is shown in Figure 4(a) shows the time series of changes in the water area from 2019 to 2021. Therefore, by analyzing the water area, the maximum water area of ISW was equal to 1953.31km². It happened in the Winter of 2019 and the minimum water area was 563.5km², which happened in the fall of 2021 (Figure 4 (b and c)). To further investigate the trend of water level changes in ISW, water body surface regression analysis was performed. The fixed number in the basic equation of water level and slope indicates the rate of decrease in water level of ISW during three years.

4.3 Seasonal WE analysis of ISW from 2019 to 2021

To investigate seasonally, The Months determined March-May as the season of Spring, June-August as the season of Summer, September-November as the season of Autumn, and December February as the season of Winter. Figure 5, illustrates the analysis result of water changes of ISW clearly that the two models have the same result. According to Figure 5, the water seasonal area of Spring and Winter was vaster than that of Summer and Autumn overall. also, Among the seasonal maximum water area, Winter was the vastest at 1953.31km², and the smallest was in Summer at 1445.72km². moreover, for the seasonal minimum water area, Winter is the vastest at 1604.56km², and Autumn is the smallest at 563.56km². further, Among the seasonal mean area, Winter was the vastest at 1829.13km², and Autumn was the smallest at 1100.22km².

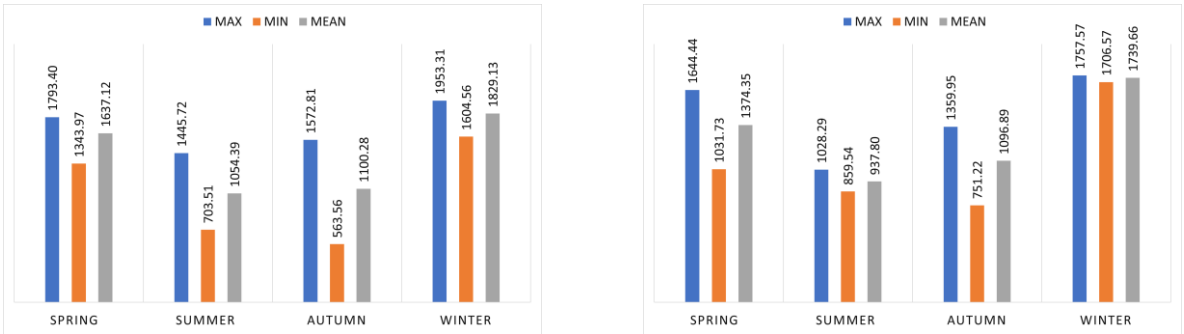

(a) (b)

Figure 5. Seasonal Mean, Maximum, and Minimum water area in ISW during 2019-2021 for (a) HA and (b) RF models.

According to the trend chart of each season in Figure 6, the water area of each season showed a decrease rate, in which the water surface area declined rapidly in Autumn, followed by Summer, Spring, and the Winter water surface area declined slowest. Overall, the downward trend in Summer and Autumn was more than that in Spring and Winter, which was also consistent with the time series water change features.

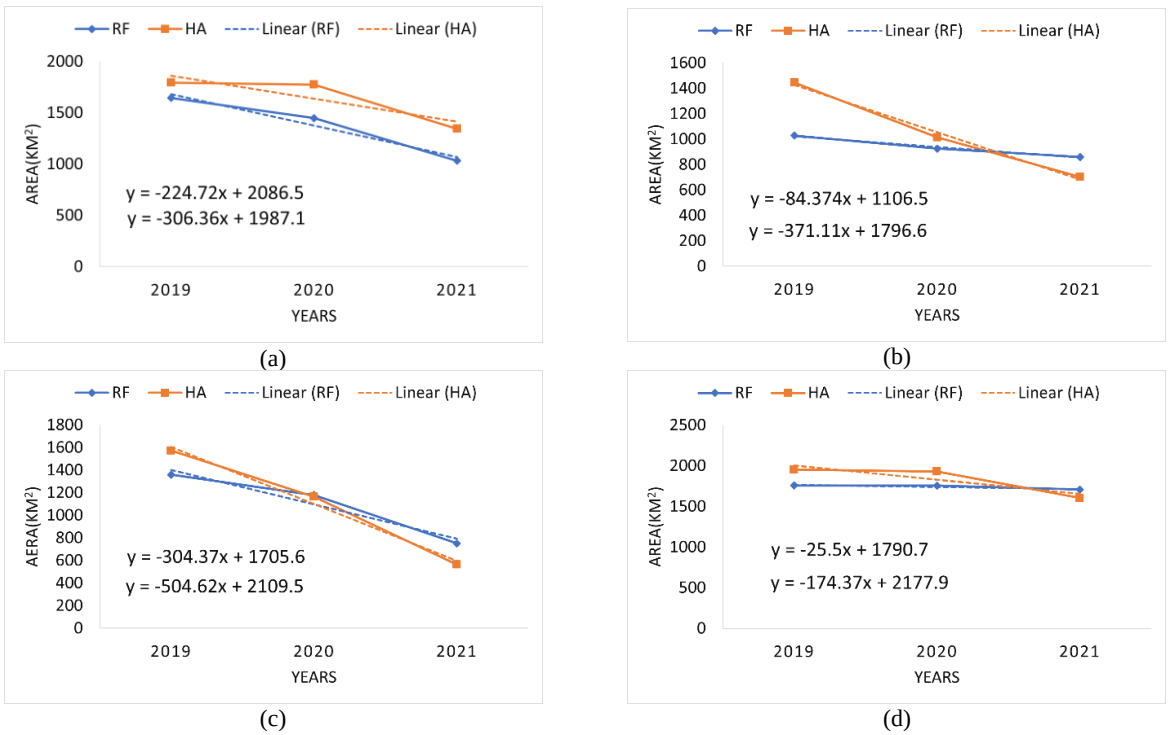

(a) (b)

(c) (d)

Figure 6. Variation trend of water area in (a) Spring, (b) Summer, (c) Autumn, and (d) Winter during 2019-2021 for HA and RF Models.

4.4 Yearly WE analysis of ISW 2019 to 2021

We analyzed the change in the maximum and minimum extents of the water body of ISW in each natural year from 2019 to 2021 (Figure 4). Through analysis, it was found that the largest water body in each natural year appeared on, 2019 (Winter), 2020 (Winter), and 2021 (Winter); the smallest water bodies appeared on, 2019 (Summer), and 2020 (Autumn), 2021 (Autumn). Therefore, it can be concluded that the largest water body generally appears in the Winter period of the year, from December to February of the following year; the smallest water body appears in the fall of the year, from September to November.

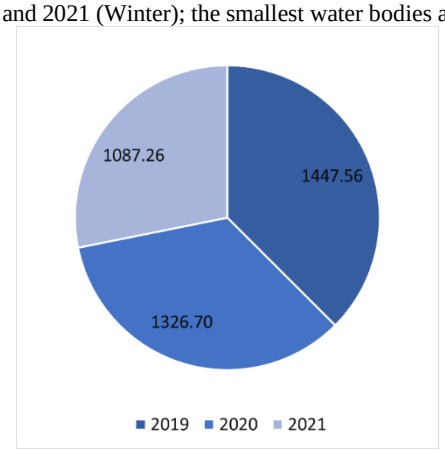

(a)

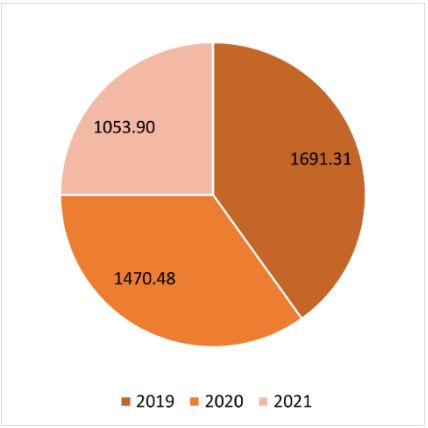

(b)

Figure 7. Mean water area changes in ISW for each year from 2019 to 2021 for (a) RF and (b) HA models. According to (a) Analyzing the annual changes, the water area of the wetland is decreasing, so that the average water area in 2019 was equal to 1447.56km², which in 2020 and 2021 decreased by 9% and 25%, respectively. And the average area of water area in these years has reached 1326.7km² and 1087.26km².

5. CONCLUSION

Using the GEE platform, we developed an automatic water extraction framework using Sentinel 2 images and the HA and analysed WE changes in ISW Wetland from 2019 to 2021. We were able to quickly and accurately explore the spatiotemporal characteristics of ISW and discuss the possible mechanisms driving these changes. In general, this study can draw the following conclusions:

1. One of the challenges of studying the changes in the WE over the years is the lack of in-situ data for labelling and training supervised classification models. According to the results, the unsupervised model of HA was compared with the supervised RF model that requires training data, and the averages of OA, Kappa, F1, and Recall parameters were calculated for each of the methods. The results show that the proposed method was able to model the changes in the WE with satisfactory accuracy. Therefore, it can be used to monitor the spatiotemporal changes in the water bodies without the need for massive training data.
2. The ISW watershed showed a relatively sharp downward trend over three years from early 2019 to late 2021. the average water body area was 1405.23km². Among them, the water area of ISW reached its peak due to the water supply to ISW Wetlands through the Jarahi River and upstream reservoirs at the end of 2019 and the beginning of 2020, and the largest water body appeared in Winter 2019, reaching 1953.31km ². In contrast, the smallest water body appeared in Autumn 2021, reaching 563.56km².
3. The ISW water body showed predictable seasonal characteristics. The water area in Winter was the largest, with an average value of 1829.13km², while the water area was the smallest in Summer, with an average value of 1100.28km². The high volume of water in Winter and Spring indicates that in general, the wetland uses the rainfall in these two seasons and upstream reservoirs to maintain its life, and in Spring and Summer due to the high temperature of the region and the use of wetland water for agricultural irrigation loses a large volume of wetland water.
4. In short, according to the Figure 4. and analysis of the characteristics of the temporal and spatial changes, it can be deduced that the water area of the lagoon is declining annually and seasonally during these three years (2019-2021), hence relying on seasonal rainfall and upstream reservoirs of the wetland, in the long run, can't be a good solution for the survival of the wetland.

REFERENCES

Adeli, S., Quackenbush, L.J., Salehi, B., Mahdianpari, M., 2022. THE IMPORTANCE OF SEASONAL TEXTURAL FEATURES FOR OBJECT-BASED CLASSIFICATION OF WETLANDS : NEW YORK STATE CASE STUDY XLIII, 6–11.

Aghdami-Nia, M., Shah-Hosseini, R., Rostami, A., Homayouni, S., 2022. Automatic coastline extraction through enhanced sea-land segmentation by modifying Standard U-Net. *Int. J. Appl. Earth Obs. Geoinf. 109, 102785.* https://doi.org/10.1016/J.JAG.2022.102785

Almasi, H., Takdastan, A., Jaafarzadeh, N., Babaei, A.A., Tahmasebi Birgani, Y., Cheraghian, B., Saki, A., Jorfi, S., 2020. Spatial distribution, ecological and health risk assessment and source identification of atrazine in Shadegan international wetland, Iran. *Mar. Pollut. Bull. 160, 111569.* https://doi.org/10.1016/j.marpolbul.2020.111569

Carroll, M.L., Townshend, J.R., DiMiceli, C.M., Noojipady, P., Sohlberg, R.A., 2009. A new global raster water mask at 250 m resolution. *Int. J. Digit. Earth 2, 291–308.* https://doi.org/10.1080/17538940902951401

Emami, H., Zarei, A., 2021. Modelling lake water's surface changes using environmental and remote sensing data: A case study of lake urmia. *Remote Sens. Appl. Soc. Environ. 23, 100594.* https://doi.org/10.1016/j.rsase.2021.100594

Fekri, E., Latifi, H., Amani, M., Zobeidinezhad, A., 2021. A training sample migration method for wetland mapping and monitoring using sentinel data in google earth engine. *Remote Sens. 13, 1–33.* https://doi.org/10.3390/rs13204169

Gao, Y., Liang, Z., Wang, B., Wu, Y., Wu, P., 2018. Wetland Change Detection Using Cross-Fused-Based and Normalized Difference Index Analysis on Multitemporal Landsat 8 OLI. *J. Sensors 2018.* https://doi.org/10.1155/2018/8130470

Gorelick, N., Hancher, M., Dixon, M., Ilyushchenko, S., Thau, D., Moore, R., 2017. Google Earth Engine: Planetary-scale geospatial analysis for everyone. *Remote Sens. Environ. 202, 18–27.* https://doi.org/10.1016/j.rse.2017.06.031

Huang, S., Li, J., Xu, M., 2012. Water surface variations monitoring and flood hazard analysis in Dongting Lake area using long-term Terra/MODIS data time series. *Nat. Hazards 62, 93–100.* https://doi.org/10.1007/s11069-011-9921-6

Hui, F., Xu, B., Huang, H., Yu, Q., Gong, P., 2008. International Journal of Remote Modelling spatial temporal change of Poyang Lake using multitemporal Landsat imagery. *Int. J. Remote Sens. 29, 5767–5784.*

Jiang, W., Ni, Y., Pang, Z., Li, X., Ju, H., He, G., Lv, J., Yang, K., Fu, J., Qin, X., 2021. An effective water body extraction method with new water index for sentinel-2 imagery. *Water (Switzerland) 13.* https://doi.org/10.3390/w13121647

Kang, S., Lee, G., Togtokh, C., Jang, K., 2015. Characterizing regional precipitation-driven lake area change in Mongolia. *J. Arid Land 7, 146–158.* https://doi.org/10.1007/s40333-014-0081-x

Li, Q., Lu, L., Wang, C., Li, Y., Sui, Y., Guo, H., 2015. MODIS-derived spatiotemporal changes of major lake surface areas in Arid Xinjiang, China, 2000-2014. *Water (Switzerland) 7, 5731–5751.* https://doi.org/10.3390/w7105731

Li, W., Qin, Y., Sun, Y., Huang, H., Ling, F., Tian, L., Ding, Y., 2016. Estimating the relationship between dam water level and surface water area for the Danjiangkou Reservoir using Landsat remote sensing images. *Remote Sens. Lett. 7, 121–130.* https://doi.org/10.1080/2150704X.2015.1117151

Magsar, A., Matsumoto, T., Enkhbold, A., Nyam-Osor, N., 2021. Application of Remote Sensing and GIS Techniques for the Analysis of Lake Water Fluctuations: A Case Study of Ugii Lake, Mongolia. *Nat. Environ. Pollut. Technol. 20, 2051–2059.* https://doi.org/10.46488/NEPT.2021.V20I05.022

Noi Phan, T., Kuch, V., Lehnert, L.W., 2020. Land cover classification using google earth engine and random forest classifier-the role of image composition. *Remote Sens. 12.* https://doi.org/10.3390/RS12152411
Pekel, J.F., Cottam, A., Gorelick, N., Belward, A.S., 2016. High-resolution mapping of global surface water and its long-term changes. *Nature 540, 418–422.* https://doi.org/10.1038/nature20584

Ranjbar, S., Zarei, A., Hasanlou, M., Akhoondzadeh, M., Amini, J., Amani, M., 2021. Machine learning inversion approach for soil parameters estimation over vegetated agricultural areas using a combination of water cloud model and calibrated integral equation model. https://doi.org/10.1117/1.JRS.15.018503 15, 018503. https://doi.org/10.1117/1.JRS.15.018503

Rokni, K., Ahmad, A., Selamat, A., Hazini, S., 2014. Water feature extraction and change detection using multitemporal landsat imagery. *Remote Sens. 6, 4173–4189.* https://doi.org/10.3390/rs6054173

Rostami, A., Akhoondzadeh, M., Amani, M., 2022a. A fuzzy-based flood warning system using 19-year remote sensing time series data in the Google Earth Engine cloud platform. *Adv. Sp. Res.* https://doi.org/10.1016/J.ASR.2022.06.008

Rostami, A., Shah-Hosseini, R., Asgari, S., Zarei, A., Aghdami-Nia, M., Homayouni, S., 2022b. Active Fire Detection from Landsat-8 Imagery Using Deep Multiple Kernel Learning. *Remote Sens. 2022, Vol. 14, Page 992 14, 992.* https://doi.org/10.3390/RS14040992

Ryu, J.H., Won, J.S., Min, K.D., 2002. Waterline extraction from Landsat TM data in a tidal flat a case study in Gomso Bay, Korea. *Remote Sens. Environ. 83, 442–456.* https://doi.org/10.1016/S0034-4257(02)00059-7

Seyed Mousavi, S.M., Akhoondzadeh Hanzaei, M., 2022. Monitoring and Prediction of the changes in water zone of wetlands using an intelligent neural-fuzzy system based on data from Google Eearth Engine system (Case study of Anzali Wetland, 2000-2019). *Eng. J. Geospatial Inf. Technol. 9, 19–42.*

Sun, F., Sun, W., Chen, J., Gong, P., 2012. Comparison and improvement of methods for identifying waterbodies in remotely sensed imagery. *Int. J. Remote Sens. 33, 6854–6875.* https://doi.org/10.1080/01431161.2012.692829

Tamiminia, H., Salehi, B., Mahdianpari, M., Quackenbush, L., Adeli, S., Brisco, B., 2020. Google Earth Engine for geo-big data applications: A meta-analysis and systematic review. *ISPRS J. Photogramm. Remote Sens. 164, 152–170.* https://doi.org/10.1016/j.isprsjprs.2020.04.001

Wang, C., Jiang, W., Deng, Yue, Ling, Z., Deng, Yawen, 2022. Long Time Series Water Extent Analysis for SDG 6.6.1 Based on the GEE Platform: A Case Study of Dongting Lake. *IEEE J. Sel. Top. Appl. Earth Obs. Remote Sens. 15, 490–503.* https://doi.org/10.1109/JSTARS.2021.3088127

Work, E.A., Gilmer, D.S., 1976. Utilization of Satellite Data for Inventorying Prairie Ponds and Lakes. *Photogramm. Eng. Remote Sensing 42, 685–694.*

Xu, H., 2006. Modification of normalised difference water index (NDWI) to enhance open water features in remotely sensed imagery. *Int. J. Remote Sens. 27, 3025–3033.* https://doi.org/10.1080/01431160600589179

Yang, Z.M., Han, L.F., Liu, Q.P., Li, C.H., Pan, Z.Y., Xu, K., 2022. Spatial and Temporal Changes in Wetland in Dongting Lake Basin of China under Long Time Series from 1990 to 2020. *Sustain. 14.* https://doi.org/10.3390/su14063620